Supporting information for review

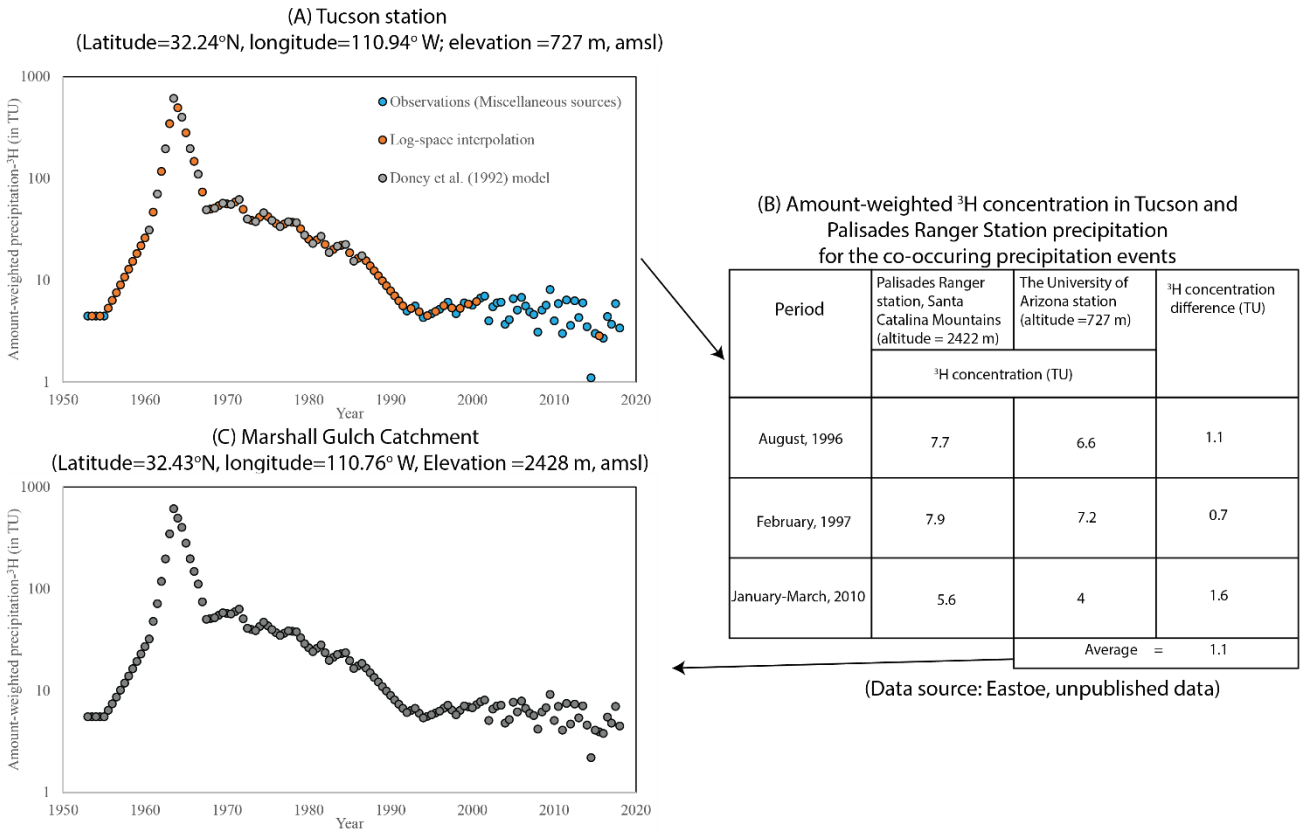

Period	Palisades Ranger station, Santa Catalina Mountains (altitude = 2422 m)	The University of Arizona station (altitude =727 m)	³H concentration difference (TU)
	³H concentration (TU)		
August, 1996	7.7	6.6	1.1
February, 1997	7.9	7.2	0.7
January-March, 2010	5.6	4	1.6
		Average =	1.1

(Data source: Eastoe, unpublished data)

Figure S1. (A) Amount-weighted ^{3}H concentration time series in Tucson precipitation from various sources, (B) difference in the observed amount-weighted ^{3}H concentrations in precipitation between Tucson and Palisades Ranger station, Santa Catalina Mountains, during co-occurring precipitation events (Data source: Dr. C. Eastoe, unpublished data), and (C) the amount-weighted ^{3}H concentration time series at MGC. Note: (i) the observed (in blue points) amount-weighted ^{3}H concentrations in (A) are obtained from Eastoe et al. (2004), the University of Arizona Environmental Isotope Laboratory rain ^{3}H concentration database (access date: September 26, 2017), and Dr. C. Eastoe, unpublished data. (ii) the modeled (orange triangle) amount-weighted ^{3}H concentrations in precipitation are based on the Doney et al. (1992) model. (iii) Interpolated values (in hollow squares) are based on the log-space linear interpolation between either observed or modeled values on a 0.5-year time scale.

Table S1. ^{3}H concentrations in streamflow and from Pigeon Spring. Note that data collected on multiple occasions and for multiple sites in the same months are averaged e.g., streamflow samples on 9/7/2017 and 9/25/2017; streamflow and Pigeon spring samples collected on 4/26/2018.

Date	^{3}H concentration in (TU)		Location	Data Source
	mean	One standard deviation		
6/15/2009	3.6	0.35	Streamflow	Ajami et al. (2011)
4/28/2016	2.6	0.35	Streamflow	The current study
9/2/2016	4.1	0.27	Streamflow	
2/2/2017	3	0.22	Streamflow	
4/27/2017	3.1	0.29	Streamflow	
9/7/2017	2.8	0.2	Streamflow	
9/25/2017	2.4	0.21	Streamflow	
4/26/2018	1.9	0.2	Streamflow	
6/1/2017	2.5	0.2	Pigeon spring	
8/18/2017	3.3	0.22	Pigeon spring	
10/20/2017	3.2	0.32	Pigeon spring	
4/26/2018	2.5	0.21	Pigeon spring	
5/17/2018	2.6	0.21	Pigeon spring	

S1. Comparison of the amplitude ratio of output to input flux cycles at various periods

Following the mathematical development (Equation 8 in the main text), the expression for the outflow tracer flux for any period λ (note: $\omega=2\pi/\lambda$) is:

$$QC(t) = \int_0^\infty (A_P(\lambda)\sin(\omega(t-\tau) - \phi_P(\lambda)) + K_P(\lambda))e^{-\kappa\tau}h(\tau)d\tau \qquad \text{(S1)}$$

If the transit time distribution *h(τ)* is an exponential type distribution with the mean transit time or mTT of β in the form of Equation (S2):

$$h(\tau) = \frac{1}{\beta}\exp\left(-\frac{\tau}{\beta}\right) \qquad \text{(S2)}$$

then Equation (S1) can be solved analytically:

$$QC(t) = \frac{A_P(\lambda)}{\sqrt{(1+\kappa\beta)^2+(\omega\beta)^2}}\sin\left(\omega t - \phi_P(\lambda) - tan^{-1}\left(\frac{\omega\beta}{1+\kappa\beta}\right)\right) + \frac{K_P(\lambda)}{1+\kappa\beta} \qquad \text{(S3)}$$

A comparison of Equation (S3) with Equation (S4) below, representing tracer flux in outflow as a sinusoidal cycle, leads to Equation (S5) for the amplitude ratio of tracer flux cycles in outflow to inflow for any period λ:

$$QC(t) = A_Q(\lambda)\sin\left(\frac{2\pi}{\lambda}t - \phi_Q(\lambda)\right) + K_Q(\lambda) \qquad \text{(S4)}$$

$$\frac{A_Q(\lambda)}{A_P(\lambda)} = F_{yw}(\lambda) = \frac{1}{\sqrt{(1+\kappa\beta)^2+(\omega\beta)^2}} \qquad \text{(S5)}$$

Additionally, in the present case where *h(τ)* is an Exponential TTD, the analytical expression for T_{yw} is:

$$T_{yw} = \beta\, log_e\left(\frac{\sqrt{(1+\kappa\beta)^2+(\omega\beta)^2}}{\sqrt{(1+\kappa\beta)^2+(\omega\beta)^2}-1}\right) \qquad \text{(S6)}$$

A comparison of the amplitude ratios for various periods suggests that the ratios obtained using Equation (11) in the main text and Equation (S5) above are the same for both conservative (e.g., $\delta^{18}O$) and non-conservative (e.g., ^3H) tracers (Figures S2A and S2B). Note that the ranges of periods considered for the two tracers are different in Figure S2. Specifically, for the $\delta^{18}O$ tracer, periods range from 2 days, which is based on the median daily sampling interval for stable water isotopes in precipitation and stream water at MGC, to 5 years, which is the maximum period that can be addressed using the present dataset (Dwivedi et al., 2021). In contrast, the periods considered for the ^3H tracer range from 1 year, based on half-yearly sampling for ^3H in Tucson precipitation, to 27 years, which corresponds to the extent of the dataset for ^3H in Tucson precipitation, 1992 to 2018 (Figure S1 above).

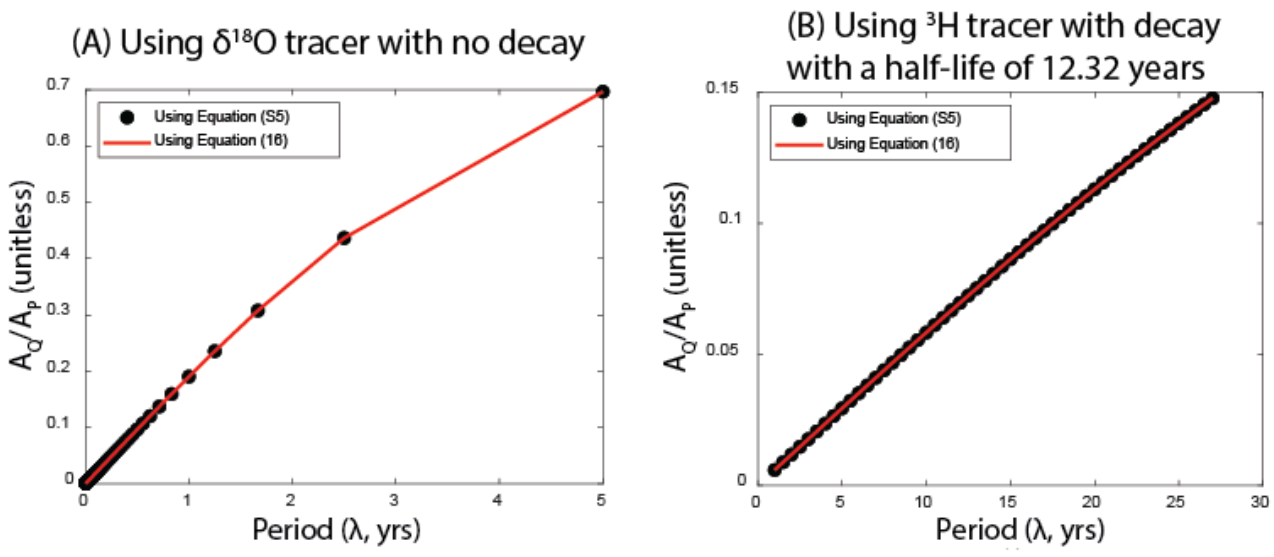

Figure S2. (A) Comparison of the amplitude ratio of tracer flux in outflow and inflow for a conservative tracer, and (B) the amplitude ratio of tracer concentration in outflow and inflow for a radioactively decaying tracer when using Equation (16) in the main text (shown here in red line) and Equation (S5) (filled points) for an exponential TTD. The TTD parameters are (A) α = 1 and β = 0.82 years and (B) α = 1 and β = 27 years for (B).

S2. Broader context for the threshold age for young water (T_{yw})

In the recent literature, Kirchner (2016) and Stewart et al. (2017) have suggested different expressions for T_{yw} when using stable water isotopes and tritium tracers, respectively. Specifically, Kirchner (2016) has suggested the use of Equation (S7) below for estimating T_{yw} for any period λ when the Gamma TTD shape parameter α is known. In contrast, Stewart et al. (2017) recommended a constant value of T_{yw} = 18 years when using the ^3H tracer with the known Gamma TTD shape parameter α ranging from 1 to 10:

$$T_{yw} \approx \lambda(0.0949 + 0.1065\alpha - 0.0126\alpha^2) \qquad \text{(S7)}$$

A comparison of T_{yw} estimated using Equation (S7), Equation (12), and Equation (S6) for an exponential TTD suggests that the patterns are very similar and yield comparable values of T_{yw} for any λ for both Exponential and Gamma TTDs (see Figure S3A for an exponential TTD and Figure S3B for a Gamma TTD).

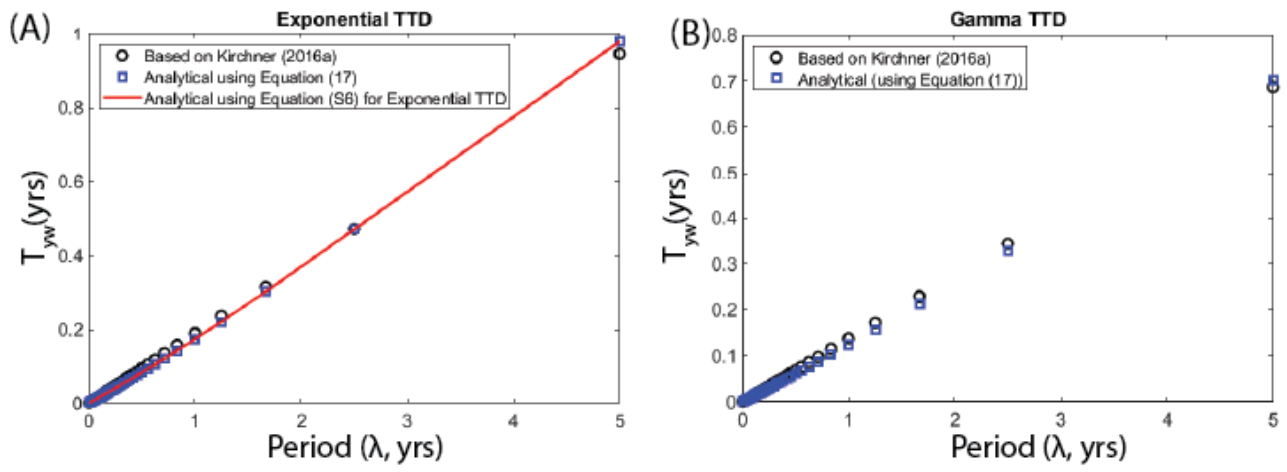

Figure S3. (A) Comparison of T_{yw} estimated using: (i) Equation (S7) (Equation (14) in Kirchner (2016); black hollow points), (ii) Equation (17) (hollow blue squares), and (iii) the analytical solution of Equation (S6) (solid red line) at various periods for an Exponential TTD. (B) Comparison of T_{yw} estimated using: (i) Equation (14) in Kirchner (2016) (black hollow points) and (ii) Equation (17) (hollow blue squares) at various periods for a Gamma TTD. The TTD parameters are set to (A) α = 1 and β = 0.82 years for and (B) α = 0.42 and β = 1.95 years for (B).

In contrast to the stable water isotope T_{yw} values, the T_{yw} values differed significantly from their analytical solutions when calculated for ^{3}H and from recommendations from Stewart et al. (2017), respectively (Figure S4A for an exponential TTD and Figure S4B for a Gamma TTD). Note that the variable λ does not appear in Stewart et al. (2017)'s recommendations for T_{yw}. Therefore, it is fair to question whether T_{yw} should be a period-invariant parameter when using the ^{3}H tracer. To address this, we considered additional cases with α varying from 1 to 10 i.e., the range considered in Stewart et al. (2017). However, only tracer cycles with λ = 1 yr were considered to represent the simplest case for T_{yw} as a function of λ. For these additional tests, even when λ = 1 yr tracer cycles are considered, the constant value of T_{yw} as a function of α is far from the analytical values calculated here (Figure S5). For example, whereas Stewart et al. (2017) proposed a constant T_{yw} (=18 years) for α between 1 to 10, it is 0.16 years for α = 1 and 0.74 years for α = 10 when using the proposed analytical solution from this work, i.e., Equation (12) in the main text. We thus endorse the use of the analytical solution-based T_{yw} values, which are obtained using Equation (12) in the main text, as T_{yw} values obtained using this method for a conservative tracer match the literature-reported pattern in T_{yw} for various periods (see Figure S3 above).

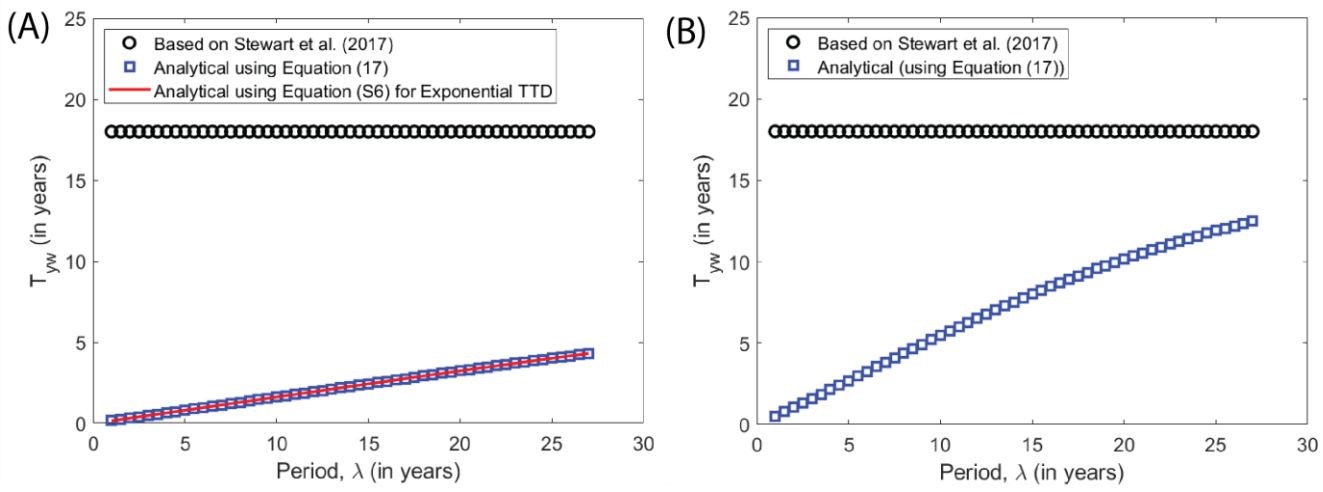

Figure S4. (A) Comparison of T_{yw} values: (i) recommended by Stewart et al. (2017) (black hollow points), (ii) estimated using Equation (17) (hollow blue square), and (iii) estimated using the analytical solution of Equation (S6) (solid red line) as a function of λ for an Exponential TTD. (B) Comparison of T_{yw} values: (i) recommended by Stewart et al. (2017) (black hollow points) and (ii) estimated using Equation (17) in the main text (hollow blue squares) as a function of λ for a Gamma TTD. The TTD parameters are set to (A) α = 1 and β = 27 years and (B) α = 6.53 and β = 4.13 years for (B).

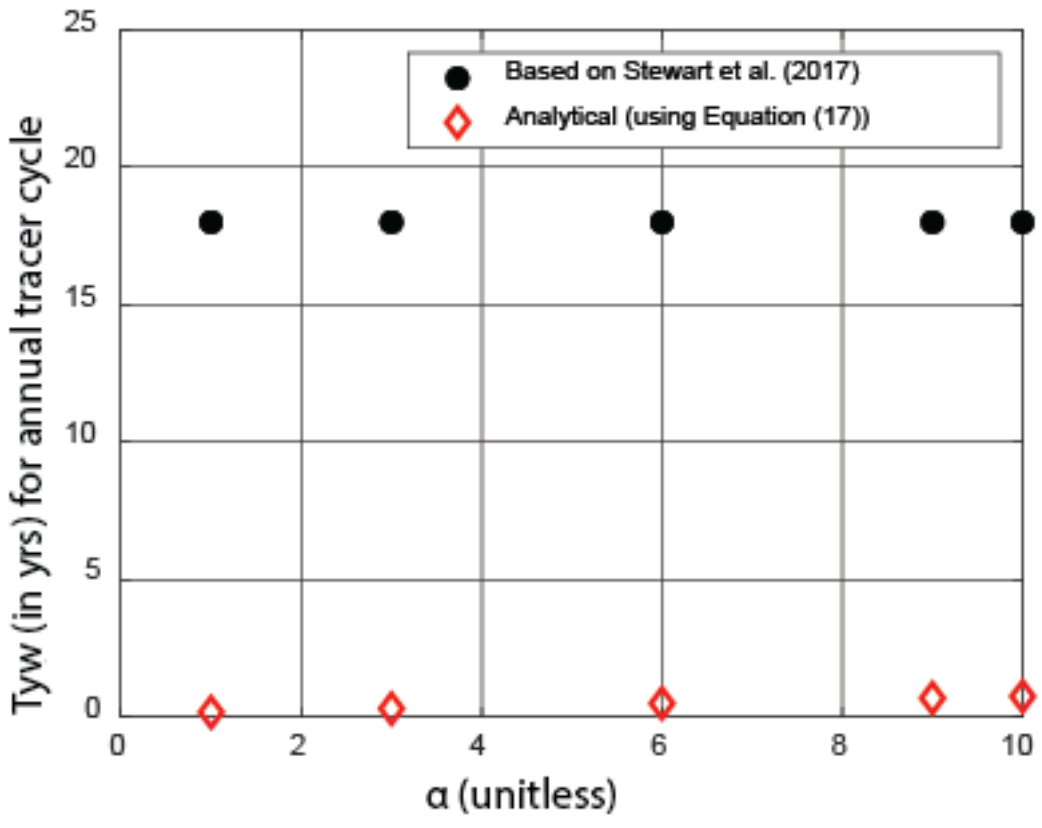

Figure S5. T_{yw} as a function of the α parameter using a Gamma TTD and the ^{3}H tracer with λ = 1 year (annual tracer cycle). The mean age for the Gamma TTD is set to 27 years.

S3. Impact of ^{3}H concentration uncertainty on estimated TTD type and parameters

Additional tests were conducted to better understand how uncertainty in amount-weighted precipitation and stream water ^{3}H concentrations affected both TTD type and its parameters. In these tests, various combinations of uncertainty in amount-weighted precipitation and stream water ^{3}H concentrations were considered with respect to their means (μ) ± one standard deviation (σ) (see Figure 3) i.e., μ – σ, μ, and μ + σ were specifically related to three possible cases of deep groundwater ^{3}H concentration uncertainty (Case #1 through Case #9 in Table S2). Subsequently, both TTD type and TTD parameters were objectively estimated using the modified Kling-Gupta efficiency (KGE') for piston flow, exponential, gamma, one-dimensional advection-dispersion (ADE-1x), and multi-dimensional advection-dispersion (ADE-nx) TTD types. The same allowable parameter space for all model parameters was used to evaluate the most suitable TTD type and parameters (Section 3.1.2). Due to the identified approximate equifinality in model parameters (Section 4.1.1) and the rough response surfaces for certain TTD types (see Figure 5), TTD model parameters were estimated from three separate model runs (Table S3).

Table S2. Cases considered for evaluating the impacts of uncertainty in precipitation and stream water ^{3}H concentrations on TTD type and its parameters. Note: μ is the mean age and σ is one standard deviation.

Case #	Precipitation	Stream water
1	μ-σ	μ-σ
2	μ-σ	μ
3	μ-σ	μ+σ
4	μ	μ-σ
5	μ	μ
6	μ	μ+σ
7	μ+σ	μ-σ
8	μ+σ	μ
9	μ+σ	μ+σ

Results of this sensitivity analysis showed that piston flow-based mTTs were always within the permissible parameter space, but there were notable differences in the estimated mTTs among model runs. For example, in Case #9, the mTT varied from 7 years to 33 years. There was also a large range in the coefficients of variation (σ / μ) resultant from piston flow-based mTT analysis between 0.02 (Case #7) and 0.96 (Case #9). Except for Case #1, mTT for the exponential TTD was always between 1 and 50 years at the higher end of the permission parameter space. The mTTs and α parameters for the gamma TTD were quite stable among the three separate model runs in all sensitivity scenarios. For the ADE-1x type, the estimated TTD model parameters fell into three categories: (1) the estimated mTTs were stable among the three separate model runs (e.g., Cases #1 and #4), but the second parameter Pe was at the higher end of the of the permissible parameter space, (2) mTT varied among model runs (e.g., Case #2) and Pe was at the higher end of the of the permissible parameter space, and (3) the estimated mTTs were stable among the three separate model runs and Pe was also stable and within the allowable parameter space (e.g., Case #6). For the ADE-nx type, the estimated second parameter Pe was always at the higher end of the allowable parameter space irrespective of scenario.

Table S3. Estimated TTD type and TTD parameters for cases listed in Table S2. PF is Piston Flow, Exp is exponential, P1 is Parameter 1 and P2 is Parameter 2.

		Run # 1			Run # 2			Run # 3		
Case #	TTD type	P1	P2	KGE'	P1	P2	KGE'	P1	P2	KGE'
	PF	28.50	0.00	0.47	30.00	0.00	0.40	30.00	0.00	0.40
	Exp	46.77	1.00	0.83	46.77	1.00	0.83	46.77	1.00	0.83
	Gamma	26.51	8.84	0.58	26.51	8.84	0.58	26.51	8.84	0.58
	ADE-1x	31.30	100.00	0.57	31.30	100.00	0.57	31.30	100.00	0.57
Case 1	ADE-nx	23.98	100.00	1.14	23.98	100.00	1.14	23.98	100.00	1.14
	PF	7.00	0.00	0.40	32.50	0.00	0.40	35.50	0.00	0.40
	Exp	50.00	1.00	0.68	50.00	1.00	0.68	50.00	1.00	0.68
	Gamma	26.91	4.28	0.55	26.91	4.28	0.55	26.91	4.28	0.55
	ADE-1x	29.13	7.52	0.56	3.79	100.00	0.42	29.13	7.52	0.56
Case 2	ADE-nx	24.38	100.00	1.06	24.38	100.00	1.06	24.38	100.00	1.06
	PF	4.00	0.00	0.27	33.00	0.00	0.41	10.50	0.00	0.28
Case 3	Exp	50.00	1.00	0.57	50.00	1.00	0.57	50.00	1.00	0.57

	Gamma	30.40	2.17	0.53	30.40	2.17	0.53	30.40	2.17	0.53
	ADE-1x	46.97	2.24	0.53	3.98	100.00	0.40	3.98	100.00	0.40
	ADE-nx	24.74	100.00	1.06	24.74	100.00	1.06	24.74	100.00	1.06
	PF	19.50	0.00	0.44	7.00	0.00	0.59	30.00	0.00	0.42
	Exp	50.00	1.00	0.87	50.00	1.00	0.87	50.00	1.00	0.87
	Gamma	26.37	11.19	0.58	26.37	11.19	0.58	26.37	11.19	0.58
	ADE-1x	30.76	100.00	0.57	30.76	100.00	0.57	30.76	100.00	0.57
Case 4	ADE-nx	24.13	100.00	1.22	24.13	100.00	1.22	24.13	100.00	1.22
	PF	32.50	0.00	0.40	29.50	0.00	0.39	35.50	0.00	0.40
	Exp	50.00	1.00	0.72	50.00	1.00	0.72	50.00	1.00	0.72
	Gamma	26.34	5.23	0.56	26.34	5.23	0.56	26.34	5.23	0.56
	ADE-1x	3.63	100.00	0.48	3.63	100.00	0.48	27.69	9.51	0.56
Case 5	ADE-nx	24.44	100.00	1.13	24.44	100.00	1.13	24.44	100.00	1.13
	PF	33.00	0.00	0.41	4.00	0.00	0.34	33.00	0.00	0.41
	Exp	50.00	1.00	0.59	50.00	1.00	0.59	50.00	1.00	0.59
	Gamma	27.80	2.74	0.53	27.80	2.74	0.53	27.80	2.74	0.53
	ADE-1x	35.35	3.72	0.53	35.35	3.72	0.53	35.35	3.72	0.53
Case 6	ADE-nx	24.69	100.00	1.11	24.69	100.00	1.11	24.69	100.00	1.11
	PF	30.00	0.00	0.45	29.00	0.00	0.47	30.00	0.00	0.45
	Exp	50.00	1.00	0.91	50.00	1.00	0.91	50.00	1.00	0.91
	Gamma	26.44	14.58	0.58	26.44	14.58	0.58	26.44	14.58	0.58
	ADE-1x	30.19	100.00	0.58	30.19	100.00	0.58	30.19	100.00	0.58
Case 7	ADE-nx	24.28	100.00	1.30	24.28	100.00	1.30	24.28	100.00	1.30
	PF	29.76	0.00	0.38	29.76	0.00	0.38	19.50	0.00	0.43
	Exp	50.00	1.00	0.75	50.00	1.00	0.75	50.00	1.00	0.75
	Gamma	25.92	6.40	0.56	25.92	6.40	0.56	25.92	6.40	0.56
	ADE-1x	26.78	11.92	0.56	26.78	11.92	0.56	26.78	11.92	0.56
Case 8	ADE-nx	24.53	100.00	1.20	24.53	100.00	1.20	24.53	100.00	1.20
	PF	7.00	0.00	0.37	33.00	0.00	0.42	7.00	0.00	0.37
	Exp	50.00	1.00	0.62	50.00	1.00	0.62	50.00	1.00	0.62
	Gamma	26.69	3.39	0.53	26.69	3.39	0.53	26.69	3.39	0.53
	ADE-1x	30.69	5.26	0.53	3.71	100.00	0.47	30.69	5.26	0.53
Case 9	ADE-nx	24.72	100.00	1.17	24.72	100.00	1.17	24.72	100.00	1.17

S4. Sources of uncertainty for F_{yw} and T_{yw} when considering annual cycles of ^{3}H in precipitation and deep groundwater

When using the iteratively re-weighted least square (IRLS) method for F_{yw} estimation from the annual ^{3}H cycles in precipitation and deep groundwater, the estimated ratio of the amplitudes in deep groundwater to precipitation, i.e., A_Q/A_P, was significantly larger than one, which is the maximum allowed value for this ratio (Section 4.3.1). As a result, we investigated the following as potential causes of this phenomenon: (a) there was no annual tracer cycle in precipitation; or (b) the amplitude of the tracer cycle in precipitation was underestimated due to the coarse sampling interval (half-yearly); or (c) the observed tracer time series in deep groundwater was too short and/or sparse to reliably estimate A_Q. With respect to (a), the estimated amplitude of annual the tracer cycle in precipitation was 0.38±0.15 TU (Table S4) and the standard error was less than the tracer cycle amplitude; hence, the observed ^{3}H data in precipitation suggest an annual tracer cycle. With respect to (b), additional tests were conducted using synthetic perfectly sinusoidal tracer time series data with an amplitude of 1 TU and a sampling interval equivalent to the observed precipitation ^{3}H time series, but with phase angles (the parameter ϕ_P in Figure S6) varying between 0 and 360^o. The IRLS method was then used to estimate the amplitude of the resultant synthetic tracer cycle. These results (Figure S6) demonstrate that the estimated amplitude of the synthetic tracer cycle was accurately predicted for phase angles of 90^o and 270^o (the phase angle of the observed precipitation ^{3}H time series data was 90^o; Table S4), and thus that the amplitude of the annual ^{3}H cycle in precipitation was reliably estimated.

With respect to (c), the estimated amplitude of the tracer cycle when using all six observations in deep groundwater was orders-of-magnitude larger and very uncertain relative to the precipitation tracer cycle amplitude (row 3 vs. row 2 in Table S4). However, if only the last five deep groundwater observations were considered, then the estimated amplitude and its standard error were 0.94 ± 0.34 TU with a phase angle of 270^o (row 4 in Table S4). We therefore conclude that a large gap in the observed ^{3}H in deep groundwater time series led to an unreliable estimate of the tracer cycle amplitude. However, even when using the amplitude of the tracer cycle from the last five deep groundwater observations, the

A_Q/A_P ratio was still larger than unity. To further understand how the length of the observed ^3H concentration in deep groundwater time series affected the estimated tracer cycle amplitude, Equation (11) or Equation (S7) below was applied to estimate the tracer cycle amplitude ratio, i.e., A_Q/A_P, using the estimated TTD parameters for deep groundwater (α = 6.53 and mTT = 27 years; Section 4.1.1). Note that in Equation S7, ω is the angular frequency, which equals to 2π/period (in years).

$$\frac{A_Q}{A_P}(\omega) = \frac{1}{(1+\kappa\beta)^{\alpha}\left(1+\left(\frac{\omega\beta}{1+\kappa\beta}\right)^2\right)^{\frac{\alpha}{2}}} \qquad \text{(S7)}$$

For an annual tracer cycle, Equation (S7) when applied using the decay data for ^3H (Stewart et al., 2017) suggested an amplitude ratio of 5.76×10^{-10}. Thus, the amplitude of the tracer cycle was very damped as a result of the large deep groundwater mTT and practically imperceptible due to the ± 0.5 TU detection limit for ^3H (see Section 2.2.3) even if a weak annual tracer cycle may exist. Together, these results suggest that the observed tracer time series in deep groundwater was too short and sparse to reliably estimate A_Q or to estimate *Fyw* using the sinusoidal curve fitting methods to the observed ^3H tracer data in deep groundwater at MGC.

Table S4. Estimated amplitudes (in Tritium Units or TU) and phase angle (in degrees) of the annual tracer cycles in precipitation and deep groundwater at MGC.

Item	Amplitude estimate (TU)	Standard Error of the amplitude estimate (TU)	Phase angle (degrees)
Observed precipitation (1992-2018; Figure 3)	0.38	0.15	90
Observed deep groundwater 3H concentrations (all six observations; inset plot in Figure 3)	3.08E+14	1.90E+14	~0
Observed deep groundwater 3H concentrations (last five observations; inset plot in Figure 3)	0.94	0.34	270

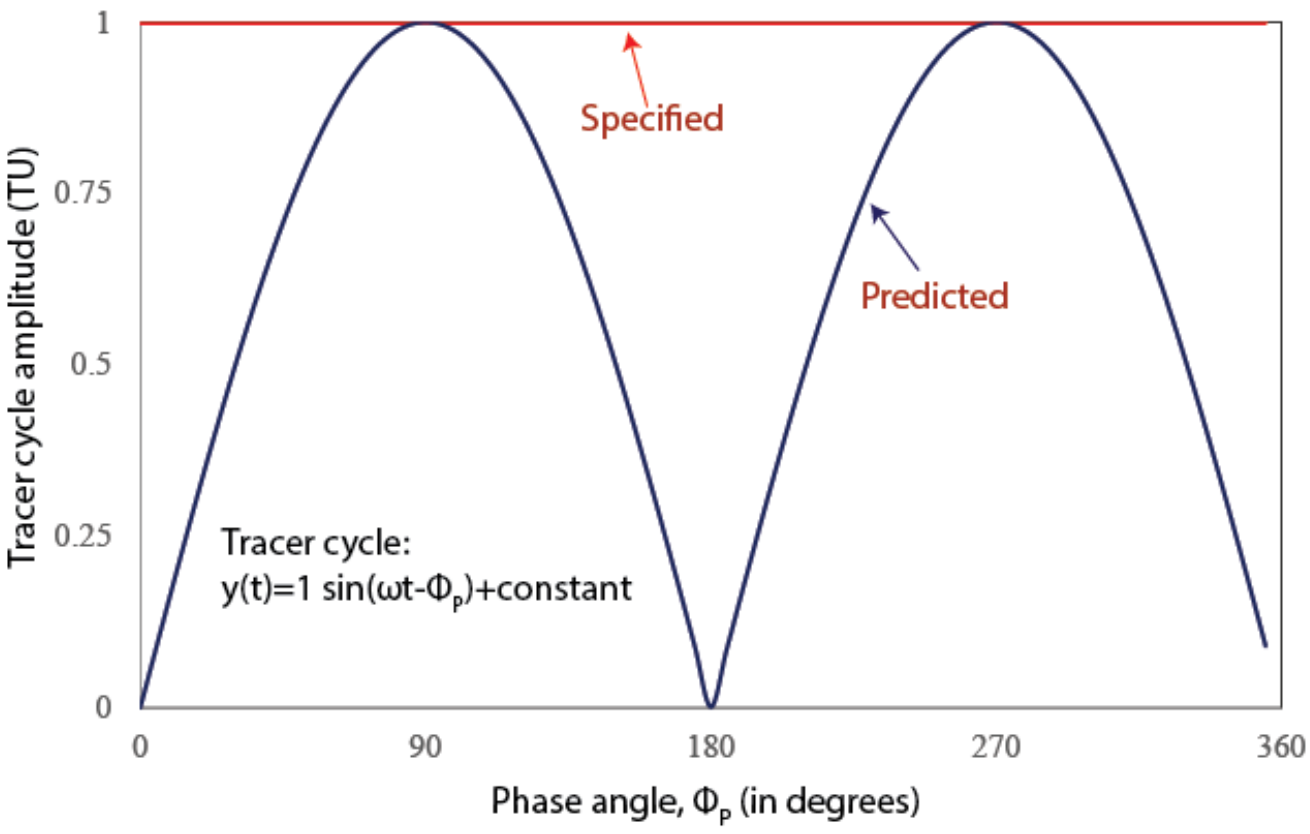

Figure S6. Specified (shown in red) and predicted amplitude of the tracer cycle for a perfectly sinusoidal tracer time series with varying phase angles.

Table S5. Estimated amplitude (second column) and its standard error (third column) for the observed ^3H concentration cycle in precipitation (A_P) for periods varying between 1 and 27 years using the iteratively re-weighted least square (IRLS) method (column #2). The ratio of amplitudes in deep groundwater to precipitation (A_Q/A_P) obtained using Equation (16) for periods varying between 1 and 27 years (column #4). The amplitude of tracer cycles in deep groundwater (A_Q) for any period is a product of A_P (second column) and A_Q/A_P (fourth column).

Period (yr)	A_P (TU)	Standard Error of A_P (TU)	A_Q/A_P (unitless)	A_Q (TU)
1	0.38	0.15	5.7E-10	2.2E-10
2	0.59	0.21	5.2E-08	3.1E-08
3	0.27	0.22	7.1E-07	1.9E-07
4	0.49	0.23	4.4E-06	2.1E-06
5	0.18	0.23	1.8E-05	3.2E-06

6	0.29	0.23	5.4E-05	1.6E-05
7	0.38	0.22	1.4E-04	5.2E-05
8	0.16	0.23	2.9E-04	4.7E-05
9	0.42	0.23	5.7E-04	2.4E-04
10	0.66	0.22	1.0E-03	6.6E-04
11	0.60	0.22	1.7E-03	1.0E-03
12	0.48	0.22	2.6E-03	1.2E-03
13	0.36	0.22	3.8E-03	1.4E-03
14	0.22	0.23	5.4E-03	1.2E-03
15	0.13	0.23	7.3E-03	9.7E-04
16	0.22	0.24	9.6E-03	2.1E-03
17	0.35	0.24	1.2E-02	4.3E-03
18	0.45	0.23	1.5E-02	6.9E-03
19	0.52	0.23	1.9E-02	9.7E-03
20	0.59	0.22	2.2E-02	1.3E-02
21	0.66	0.22	2.6E-02	1.7E-02
22	0.73	0.21	3.0E-02	2.2E-02
23	0.78	0.20	3.5E-02	2.7E-02
24	0.83	0.20	3.9E-02	3.3E-02
25	0.88	0.20	4.4E-02	3.9E-02
26	0.91	0.19	4.9E-02	4.5E-02
27	0.94	0.19	5.4E-02	5.0E-02

Table S6. F_{yw}^{*} estimates reported in the current study compared to various other tracer studies (all using stable water isotopes except Wilusz et al. (2017) who used chloride) where A is the drainage area, θ is the mean topographic gradient, and F_{yw}^{*} values are for an annual tracer cycle.

Source	Study site (s)	A (sq. km)	θ (%)	F_{yw}^{*} (%)	Method	Sampling interval	Climate	Comments
This study	MGC, USA	1.55	40	34.9 (TTD-method), 11.4 (IRLS method), and 7.9 (WWT method)	Various	daily with data gaps	Sub-humid	None
von Freyberg et al. (2018)	Erlenbach, Lumpenenbach, Reitholzbach, and Vogelbach out of 22 catchments	0.7 -3.2	14.6 - 28.9	20 - 49	IRLS method	Two weeks	Humid to temperate continental climate	None
Jasechko et al. (2016)	Brugga - Oberried, DE; Botorpstrommen - Gunnebo, SE; Rietholzbach - Mosnang (Pegel), CH; McDonalds B In Lebanon State Forest, USA	2 - 6	Not provided	6 - 33	Periodic regression method of Bliss (1970) as described in Dewalle et al. (1997)	~ Monthly	Humid (Brugga - Oberried); warm and temperate (Botorpstrommen - Gunnebo); temperate humid (Rietholzbach - Mosnang (Pegel)); and humid (McDonalds B In Lebanon State Forest)	The F_{yw}^{*} range is estimated by scaling Fyw by a factor of 1.26 from von Freyberg et al. (2018). The topographic gradients are estimated from ETOPO1 global relief data with a spatial resolution of ~1 km at Equator Amante and Eakins (2009). The sampling interval is estimated from the ratio of median number of years with stream water isotope data to median number of samples.
Gallart et al. (2020)	Can Vila catchment, Spain	0.56	25.6	10.3 % (weekly sampling), 22.6 (high resolution sampling, 30.4 ("virtual thorough sampling")	Least squares fitting	30 minutes to one week, depending on flow conditions	Mediterranean sub-humid	One location for both precipitation and stream water, and both are near the outlet. They used Fyw vs. Q relationship to estimate Fyw at every 5 minute discharge observations. Subsequently Fyw values are volume weighted to estimate

								volume weighted Fyw (called Fyw based on "Virtual" thorough sampling")
Song et al. (2017)	Zuomaokong watershed, Qinghai-Tibet Plateau	10.9 (catchment # 5)	4.5	26.00	TTD-based method after estimating TTD parameters for assumed Gamma TTD type	Daily	Permafrost watershed	Only one thaw season is considered in the analysis. The F_{yw}^{*} value is estimated by scaling Fyw by a factor of 1.26 from von Freyberg et al. (2018).
Wilusz et al. (2017)	Lower Hafren and Tanllwyth, UK	0.9 - 3.5	Not provided	30 - 55	Rainfall-runoff modeling using Kirchner (2009) approach and using rank StorAge Selection function method of Harman (2015) for transit time modeling. The F_{yw}^{*} value is calculated using TTD-based method.	Weekly	Humid	None
Zhang et al. (2018)	Boulder Creek watershed, USA	0.95 - 5.56 (four nested catchments)	Not provided	8 - 28	Convolution integral method for amplitude estimation for tracer data in precipitation and stream water	Weekly	Alpine, subalpine, and Montane	The F_{yw}^{*} range is estimated by scaling Fyw by a factor of 1.26 from von Freyberg et al. (2018).
Lutz et al. (2018)	Bode catchment, Germany	0.11 - 200 (all subcatchments)	16.5 (sites in mountains)	1.3 - 19 (sites in mountains)	IRLS method for sinusoidal curve fitting to the tracer data in precipitation and ordinary least squares method for sinusoidal curve fitting to tracer data in steam water	Monthly	Cold and wet in high elevations	The F_{yw}^{*} range is estimated by scaling Fyw by a factor of 1.26 from von Freyberg et al. (2018).

Bansah and Ali (2019)	South Tobacco Creek watershed, Canada	0.19 - 1.88	Not provided	42 - 91	Sinusoidal curve fitting to tracer data in precipitation and stream water	Mostly weekly but also higher sampling frequency during storm events	Semi-arid to sub-humid	The watershed is heavily used for agriculture. The Fyw values are average of the wet and dry year values. The F_{yw}^{*} range is estimated by scaling Fyw by a factor of 1.26 from von Freyberg et al. (2018).
Clow et al. (2018)	Andrew Creek, CO, and Andrews spring, CO, out of 11 headwater catchments in the Western USA	0.1 - 1.7	85 - 102	19 - 21	Multiple regression method	Monthly	Cold and wet during winter and warm and dry during summer	Stream water isotope data were detrended before Fyw estimation. The F_{yw}^{*} range is estimated by scaling Fyw by a factor of 1.26 from von Freyberg et al. (2018).
Stockinger et al. (2017)	Wusteback headwater catchment, Germany	0.385	Not provided	13 - 16 (simple method) to 14 - 16 (complex method)	Simple (based on the amplitude ratio of tracer signal in streamflow and precipitation) and complex (based on the TTD parameters and TTD-based F_{yw}) methods	Weekly	Humid temperate	The F_{yw}^{*} range is estimated by scaling Fyw by a factor of 1.26 from von Freyberg et al. (2018).
Stockinger et al. (2019)	Wusteback headwater catchment, Germany	0.385	Not provided	5 to ~16	IRLS method	Weekly	Humid	None
Rodriguez et al. (2021)	Weierbach Catchment, Luxembourg	0.42	71% area with slope between 0-9% and 29 % area with slope between 9 to 96%	1.5	TTD-based method that uses StorAge Selection functions (more details in Rodriguez and Klaus (2019)	Sub-daily sampling for stable water isotopes and bi-weekly for tritium	Temperate and semi-oceanic	None

			(Rodriguez and Klaus (2019)					

References

Ajami, H., Troch, P. A., Maddock, T., Meixner, T., and Eastoe, C.: Quantifying mountain block recharge by means of catchment-scale storage-discharge relationships, Water Resources Research, 47, 1-14, 10.1029/2010wr009598, 2011.

Amante, C., and Eakins, B. W.: ETOPO1 1 ARC-MINUTE GLOBAL RELIEF MODEL: PROCEDURES, DATA SOURCES AND ANALYSIS NOAA, National Geophysical Data Center, Boulder, Colorado, 2009.

Bansah, S., and Ali, G.: Streamwater ages in nested, seasonally cold Canadian watersheds, Hydrological Processes, 33, 495-511, 10.1002/hyp.13373, 2019.

Bliss, C. I.: Statistics in Biology, McGraw-Hill, New York, 1970.

Clow, D. W., Mast, M. A., and Sickman, J. O.: Linking transit times to catchment sensitivity to atmospheric deposition of acidity and nitrogen in mountains of the western United States, Hydrological Processes, 32, 2456-2470, 10.1002/hyp.13183, 2018.

Dewalle, D. R., Edwards, P. J., Swistock, B. R., Aravena, R., and Drimmie, R. J.: Seasonal isotope hydrology of three Appalachian forest catchments, Hydrological Processes, 11, 1895-1906, 1997.

Doney, S. C., Glover, D. M., and Jenkins, W. J.: A model function of the global bomb tritium distribution in precipitation, 1960–1986, Journal of Geophysical Research, 97, 5481, 10.1029/92jc00015, 1992.

Dwivedi, R., Eastoe, C., Knowles, J. F., Hamann, L., Meixner, T., Ferre, P. A. T., Castro, C., Wright, W. E., Niu, G.-Y., Minor, R., Barron-Gafford, G. A., Abramson, N., Mitra, B., Papuga, S. A., Stanley, M., and Chorover, J.: An improved practical approach for estimating catchment-scale response functions through wavelet analysis, Hydrological Processes, 35, 1-20, https://doi.org/10.1002/hyp.14082, 2021.

Eastoe, C. J., Gu, A., and Long, A.: The Origins, Ages and Flow Paths of Groundwater in Tucson Basin: Results of a Study of Multiple Isotope Systems, in: Groundwater Recharge in a Desert Environment: The Southwestern United States, edited by: Hogan, J. F., Phillips, F. M., and Scanlon, B. R., American Geophysical Union, Washington, D. C., 2004.

Gallart, F., Valiente, M., Llorens, P., Cayuela, C., Sprenger, M., and Latron, J.: Investigating young water fractions in a small Mediterranean mountain catchment: Both precipitation forcing and sampling frequency matter, Hydrological Processes, 34, 3618-3634, 10.1002/hyp.13806, 2020.

Harman, C. J.: Time-variable transit time distributions and transport: Theory and application to storage-dependent transport of chloride in a watershed, Water Resources Research, 51, 1-30, 10.1002/2014WR015707, 2015.

Jasechko, S., Kirchner, J. W., Welker, J. M., and McDonnell, J. J.: Substantial proportion of global streamflow less than three months old, Nature Geoscience, 9, 126-129, 10.1038/ngeo2636, 2016.

Kirchner, J. W.: Catchments as simple dynamical systems: Catchment characterization, rainfall-runoff modeling, and doing hydrology backward, Water Resources Research, 45, 1-34, 10.1029/2008wr006912, 2009.

Kirchner, J. W.: Aggregation in environmental systems- Part 1: Seasonal tracer cycles quantify young water fractions, but not mean transit times, in spatially heterogeneous catchments, Hydrology and Earth System Sciences, 20, 279-297, 10.5194/hess-20-279-2016, 2016.

Lutz, S. R., Krieg, R., Müller, C., Zink, M., Knöller, K., Samaniego, L., and Merz, R.: Spatial Patterns of Water Age: Using Young Water Fractions to Improve the Characterization of Transit Times in Contrasting Catchments, Water Resources Research, 54, 4767-4784, 10.1029/2017wr022216, 2018.

Rodriguez, N. B., and Klaus, J.: Catchment Travel Times From Composite StorAge Selection Functions Representing the Superposition of Streamflow Generation Processes, Water Resources Research, 55, 9292-9314, 10.1029/2019wr024973, 2019.

Rodriguez, N. B., Pfister, L., Zehe, E., and Klaus, J.: Testing the truncation of travel times with StorAge Selection functions using deuterium and tritium as tracers, Hydrol. Earth Syst. Sci., 25, 401–428, 10.5194/hess-2019-501, 2021.

Song, C., Wang, G., Liu, G., Mao, T., Sun, X., and Chen, X.: Stable isotope variations of precipitation and streamflow reveal the young water fraction of a permafrost watershed, Hydrological Processes, 31, 935-947, 10.1002/hyp.11077, 2017.

Stewart, M. K., Morgenstern, U., Gusyev, M. A., and Maloszewski, P.: Aggregation effects on tritium-based mean transit times and young water fractions in spatially heterogeneous catchments and groundwater systems, and implications for past and future applications of tritium, Hydrology and Earth System Sciences, 21, 4615–4627, 10.5194/hess-21-4615-2017, 2017.

Stockinger, M. P., Lücke, A., Vereecken, H., and Bogena, H. R.: Accounting for seasonal isotopic patterns of forest canopy intercepted precipitation in streamflow modeling, Journal of Hydrology, 555, 31-40, 10.1016/j.jhydrol.2017.10.003, 2017.

Stockinger, M. P., Bogena, H. R., Lücke, A., Stumpp, C., and Vereecken, H.: Time variability and uncertainty in the fraction of young water in a small headwater catchment, Hydrology and Earth System Sciences, 23, 4333-4347, 10.5194/hess-23-4333-2019, 2019.

von Freyberg, J., Allen, S. T., Seeger, S., Weiler, M., and Kirchner, J. W.: Sensitivity of young water fractions to hydro-climatic forcing and landscape properties across 22 Swiss catchments, Hydrology and Earth System Sciences, 22, 3841-3861, 10.5194/hess-22-3841-2018, 2018.

Wilusz, D. C., Harman, C. J., and Ball, W. P.: Sensitivity of Catchment Transit Times to Rainfall Variability Under Present and Future Climates, Water Resources Research, 53, 231-256, 10.1002/2017WR020894, 2017.

Zhang, Q., Knowles, J. F., Barnes, R. T., Cowie, R. M., Rock, N., and Williams, M. W.: Surface and subsurface water contributions to streamflow from a mesoscale watershed in complex mountain terrain, Hydrological Processes, 32, 954-967, 10.1002/hyp.11469, 2018.